SCIENCE CHINA
Chemistry

•ARTICLES•

February 2022 Vol.65 No.2: 363–372
https://doi.org/10.1007/s11426-021-1157-9

Supertough spontaneously self-healing polymer based on septuple dynamic bonds integrated in one chemical group

Luzhi Zhang[1], Qingbao Guan[1], Ao Shen[1], Rasoul Esmaeely Neisiany[2], Zhengwei You[1*] & Meifang Zhu[1]

[1]*State Key Laboratory for Modification of Chemical Fibers and Polymer Materials, Shanghai Belt and Road Joint Laboratory of Advanced Fiber and Low-dimension Materials (Donghua University), College of Materials Science and Engineering, Shanghai Engineering Research Center of Nano-Biomaterials and Regenerative Medicine, Institute of Functional Materials, Donghua University, Research Base of Textile Materials for Flexible Electronics and Biomedical Applications, China Textile Engineering Society, Shanghai 201620, China;*
[2]*Department of Materials and Polymer Engineering, Hakim Sabzevari University, Sabzevar 9617976487, Iran*

Received September 15, 2021; accepted November 8, 2021; published online December 15, 2021

The development of spontaneously self-healing materials with excellent mechanical properties remains a formidable challenge despite the extensive interest in such materials. This is because the self-healing and mechanical properties of a material are usually optimized *via* contradictory routes. The present study demonstrated a supertough spontaneously self-healing polymer, Fe-(2,6-diacetylpyridine dioxime)-urethane-based polyurethane (Fe-PPOU) based on septuple dynamic bonds integrated in one chemical group. A synergistic effect was induced by the presence of multiple dynamic crosslinking points, which comprised the integrated dynamic interactions, and the hidden lengths of the folded polymeric chains in Fe-PPOU. Thus, the mechanical and self-healing properties of the polymer were simultaneously optimized. Fe-PPOU demonstrated the highest reported toughness (139.8 MJ m^{-3}) among all the room-temperature spontaneously self-healing polymers with a nearly 100% healing rate. Fe-PPOU exhibited instant (30 s) self-healing to reach a strength of 1.6 MPa that was higher than the original strength of numerous recently reported self-healing polymers.

oxime-urethane bonds, hydrogen bonds, metal-coordination bonds, 2,6-diacetylpyridine dioxime, self-healing

Citation: Zhang L, Guan Q, Shen A, Neisiany RE, You Z, Zhu M. Supertough spontaneously self-healing polymer based on septuple dynamic bonds integrated in one chemical group. *Sci China Chem*, 2022, 65: 363–372, https://doi.org/10.1007/s11426-021-1157-9

1 Introduction

The self-healing behavior of organisms in nature prevents further harm after injury, and it inspires researchers to develop self-healing materials [1–4]. The self-healing ability effectively extends the service life, increases the operational safety, and lowers the maintenance cost of the materials. Self-healing polymers have shown great promise in numerous fields such as aerospace, soft robotics, and wearable electronics, and attracted extensive attention in recent years [5–9]. They are generally designed through the introduction of reversible chemical/physical interactions in materials [10–17]. The development of room-temperature spontaneously self-healing materials is necessitated by the application and eventual damage of most materials under ambient conditions. However, most of the reversible chemical/physical groups require high energy to achieve satisfactory reversibility. Therefore, external stimuli, such as heat, light, and additional reagents, are necessary to drive the healing process of most self-healing polymers [18–21]. The realization of spontaneously self-healing polymers remains a significant challenge in the field of self-healing materials.

*Corresponding author (email: zyou@dhu.edu.cn)

To achieve room-temperature spontaneously self-healing, it is necessary to develop polymers based on dynamic bonds that exhibit reversibility at room temperature. In 2008, Cordier and coworkers [1] pioneered the synthesis of self-healing polymers based on hydrogen bonds. Thereafter, spontaneously self-healing polymers have been synthesized based on various noncovalent interactions such as hydrogen bonds [22–25], metal-ligand coordination [26,27], ionic interactions [28–30], host-guest interactions [31], and π-π stacking interactions [32]. Additionally, spontaneously self-healing has been achieved in polymers comprising dynamic covalent bonds such as disulfide bonds [33–35], boronic ester bonds [36], and urea bonds [13]. These dynamic interactions endow a material with spontaneously self-healing ability; however, the individual strengths of these interactions are relatively low. Therefore, their presence induces deterioration in the mechanical properties of the material. The toughness of most spontaneously self-healing polymers is less than 50 MJ m^{-3}, which corresponds to the toughness of extensively used natural rubber. The practical applications of self-healing polymers are limited by their poor mechanical properties.

Recently, the integration of multiple dynamic bonds in one network has been explored for the development of room-temperature self-healing polymers with excellent mechanical properties [37,38]. We proposed the development of self-healing polymers based on networks with triple dynamic bonds. Thus, both self-healing properties and mechanical properties were simultaneously optimized, and the polymer exhibited a toughness of 87.0 MJ m^{-3} [38]. Li *et al*. [39] recently demonstrated a strategy involving strain-induced crystallization for the synthesis of self-healing elastomers based on dual hydrogen bonds. The elastomer exhibited a toughness of up to 121.8 MJ m^{-3}, and this was the highest reported toughness for room-temperature spontaneously self-healing polymers. Herein, we proposed a new design of the polymer network, that is, incorporation of multiple interactions in one chemical group, not just in one network. This design minimized the number of crosslinking points formed by the predetermined number of dynamic crosslinking interactions. The fewer the crosslinking points, the higher the mobility of polymer chains, which is critical to the self-healing of the polymer. At the same time, the retained extensive dynamic crosslinking interactions ensured high energy dissipation during stretching leading to a high toughness of the polymer. Accordingly, we synthesized a supertough room-temperature self-healing polymer, Fe-(2,6-diacetylpyridine dioxime)-urethane-based polyurethane (Fe-PPOU). Fe-PPOU comprises septuple dynamic bonds integrated in one chemical group (Figure 1). The 2,6-diace-

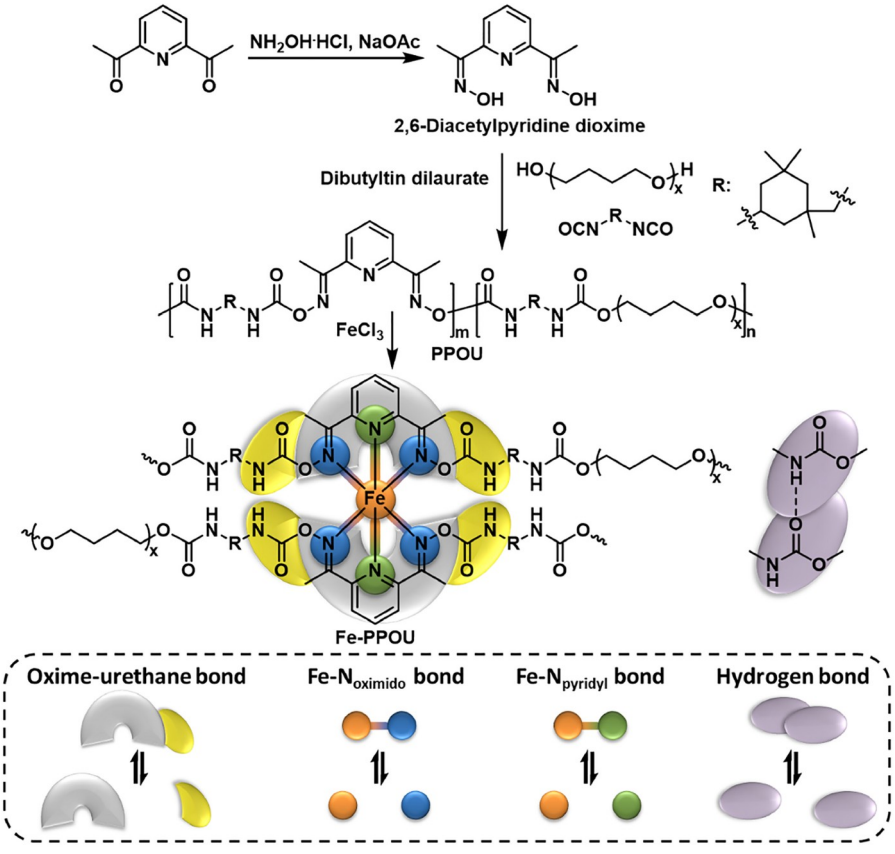

Figure 1 Schematic illustration of the design and synthesis of Fe-PPOU with septuple dynamic bonds in one chemical group (color online).

tylpyridine dioxime-urethane group contains four dynamic bonds, *i.e.*, two oxime-urethane bonds and two hydrogen bonds. Furthermore, 2,6-diacetylpyridine dioxime functioned as a ligand to coordinate with Fe ions *via* three dynamic bonds, *i.e.*, one Fe–$N_{pyridyl}$ and two Fe–$N_{oximido}$. The synergistic effect of the integration of septuple dynamic bonds in one chemical group resulted in a significant increase in the mechanical performance of the polymer. The toughness of the resultant self-healing polymer was higher than that of all the previously reported room-temperature spontaneously self-healing polymers [1,13,22–50].

2 Experimental

2.1 Materials

Polytetramethylene ether glycol (M_n ~1000 g mol^{-1}), isophorone diisocyanate (99%), and dibutyltin dilaurate (95%) were purchased from Aladdin Chemical Co., Ltd. (China). 2,6-Diacetylpyridine (98%), $NH_2OH{\cdot}HCl$ (99%), NaOAc (99%), EtOH (99.7%), acetone (99.5%), butyl isocyanate (98%), and deuterated solvents were purchased from Taitan Technology Co. Ltd. (China). $FeCl_3$ was purchased from Sinopharm Chemical Reagent Co., Ltd. (China), while anhydrous tetrahydrofuran was purchased from J&K Chemical Co., Ltd. (China). The purchased polytetramethylene ether glycol was dehydrated under vacuum at 110 °C for 2 h and then cooled to 25 °C before use.

2.2 Methods

2.2.1 Synthesis of 2,6-diacetylpyridine dioxime

2,6-Diacetylpyridine (4.895 g, 30 mmol), $NH_2OH{\cdot}HCl$ (6.254 g, 90 mmol), and NaOAc (12.304 g, 150 mmol) were added to a mixture of H_2O and EtOH (2:1, *v*/*v*). The resultant mixture was heated to 90 °C and refluxed for 2 h. Subsequently, it was cooled to 25 °C, filtered to obtain a crude product, and then washed thrice with H_2O/EtOH (4:1, *v*/*v*) for further purification. Finally, 2,6-diacetylpyridine dioxime (77% yield) was obtained as a white powder *via* drying in a vacuum oven at 30 °C over 48 h. The successful synthesis of 2,6-diacetylpyridine dioxime was confirmed by the results of Fourier transform infrared (FTIR) spectroscopy (Figure S1, Supporting Information online), nuclear magnetic resonance (NMR) spectroscopy (Figures S2, S3), and elemental analysis (Table S1, Supporting Information online).

2.2.2 Synthesis of PPOU

Polytetramethylene ether glycol (4.000 g, 4 mmol), 2,6-diacetylpyridine dioxime (0.773 g, 4 mmol), and isophorone diisocyanate (1.776 g, 8 mmol) were dissolved in 8 mL of tetrahydrofuran in a round-bottomed flask. Dibutyltin dilaurate (0.020 g) was added to the mixture and reacted for 8 h under magnetic stirring at 65 °C in an N_2 atmosphere. Thereafter, the reaction mixture was poured into a polytetrafluoroethylene mold at 45 °C, and the temperature was gradually increased to 85 °C over 15 h. Finally, PPOU (91% yield) was obtained *via* heating at 65 °C under vacuum for 24 h.

2.2.3 Synthesis of Fe-PPOU and 0.5Fe-PPOU

PPOU (0.897 g) was dissolved in acetone (9 mL) at 25 °C under magnetic stirring for 2 h. Subsequently, $FeCl_3$ (0.044 g for Fe-PPOU, 0.022 g for 0.5Fe-PPOU) was added to this mixture, and the magnetic stirring was continued for 22 h. Thereafter, the reaction mixture was poured into a polytetrafluoroethylene mold, and the solvent was evaporated over 48 h. Finally, Fe-PPOU (96% yield) or 0.5Fe-PPOU (97% yield) was obtained *via* heating at 65 °C under vacuum for 24 h.

2.2.4 General characterization

All the tests were performed at room temperature (25 °C), unless specified otherwise. The ^{1}H and ^{13}C NMR spectra were recorded using the AVANCE III 600 MHz spectrometer from Bruker BioSpin, GmbH (Germany). The FTIR spectra were recorded using the Nicolet 8700 spectrometer equipped with an ATR accessory from Thermo Fisher Scientific (USA). Dynamic mechanical analyses were performed at a DMA1 (METTLER TOLEDO) Dynamic Mechanical Analyzer. Rectangular samples were tested at a frequency of 1 Hz and a strain of 0.1%. Heating ramps of 5 °C min^{-1} were applied from −110 to 100 °C. The glass transition temperatures (T_g) were estimated from the maximum loss modulus. Stress-relaxation analysis was performed using the Exceed E42 electronic universal testing machine from MTS Systems Corporation (USA). The experiments were performed using rectangular films with thickness, width, and length of approximately 1, 3, and 20 mm, respectively, in the strain-control mode (10% strain). The temperature-dependent stress-relaxation experiments were performed in the strain-control mode (1% strain) using the ARES-G2 rotational rheometer with 25 mm diameter parallel plates from TA Instruments (USA). The relaxation modulus (G) was normalized to the initial modulus (G_0). The characteristic relaxation time (τ^*) was defined as the time required for G/G_0 to reach 1/e, according to the following exponential decay function: $G(t)=G_0\exp(-t/\tau^*)$. The apparent activation energy (E_a) was calculated using the Arrhenius equation, $\ln\tau^*(T)=\ln\tau_0+E_a/RT$. Here, τ_0, R, and T represent the characteristic relaxation time at an infinite temperature, universal gas constant, and absolute temperature, respectively. Rheological experiments were performed using the ARES-G2 rotational rheometer with 8 mm diameter parallel plates from TA Instruments (USA). Frequency sweeps were performed from 10^2 to 10^{-2} Hz at 0.1% stain at −25, −15, −5, 5, 15, 25, 35, 45,

55 and 65 °C. The master curves were built according to the time-temperature superposition principle. X-ray photoelectron spectroscopy (XPS) was performed using the Escalab 250Xi spectrometer from Thermo Fisher Scientific (USA), and the XPS profiles (N 1s and Fe 2p) were analyzed using the Avantage software package. Elemental analysis was performed using the Vario EL III analyzer from Elementar Analysensysteme GmbH (Germany). The molecular weights were measured *via* gel-permeation chromatography (GPC) using the GPC-50 system from Agilent Technologies, Inc. (USA). Here, dimethylacetamide was used as the eluent. The mechanical tests were performed using the Exceed E42 electronic universal testing machine from MTS Systems Corporation (USA). The deflection rate for the uniaxial tensile and cyclic tensile measurements was 50 mm min^{-1}. The self-healing behavior was characterized using scratch recovery tests, and the restoration of the mechanical properties was analyzed over various healing times. The scratch recovery tests were performed by scratching the films using a blade. The changes in the scratch-width track were observed *via* optical microscopy using the MDA2000 microscope from Future Optics Sci. & Tech. Co., Ltd. (China). The self-healing mechanical properties of the materials were assessed by splicing two cut specimens over specified healing durations. Processing of the polymer was carried out by cutting samples into pieces and putting the debris together for re-molding at 80 °C for 10 h.

3 Results and discussion

Firstly, NMR spectroscopy was used to monitor the reversibility formation and dissociation of oxime-urethane bonds in 2,6-diacetylpyridine dioxime-urethane group *via* small-molecule model reactions (Figures S2−S7). We mixed the 1.8:1 molar ratio of butyl isocyanate (marked as A) and 2,6-diacetylpyridine dioxime (marked as B) in DMSO-d_6 at room temperature. The reactant of A and B were marked as A-B and A-B-A, respectively. The signals at around 2.443, 2.263, and 2.256 ppm in proton nuclear magnetic resonance (^{1}H NMR) spectra corresponded to the protons of A-B-A (marked as c), A-B (marked as b) and B (marked as a), respectively (Figure S6a, b). The signals of a were disappeared within 12 h (Figure S6c), indicating almost all 2,6-diacetylpyridine dioxime participated in the reaction. The molar fraction of A-B and A-B-A reached equilibrium within 40 h (Figure S6d), indicating the formation of 2,6-diacetylpyridine dioxime-urethane group. Similarly, we dissolved A-B-A in DMSO-d_6. The molar fraction of A-B increased with time, indicating the dissociation of 2,6-diacetylpyridine dioxime-urethane group (Figure S7). These results demonstrated the reversibility of oxime-urethane bonds in 2,6-diacetylpyridine dioxime-urethane group at room temperature.

Fe-PPOU was synthesized in three steps from commercially available reagents (Figure 1). Firstly, 2,6-diacetylpyridine dioxime was prepared by one-step reaction from 2,6-diacetylpyridine. Secondly, PPOU was synthesized *via* a one-pot polycondensation reaction between polytetramethylene ether glycol, isophorone diisocyanate, and 2,6-diacetylpyridine dioxime. Polytetramethylene ether glycol comprises a flexible polymer chain, while isophorone diisocyanate possesses a loose structure and inhibits crystallization. Both facilitate the motion of polymer chains and contribute to the self-healing ability of the materials. The activation of the reversible dissociation of derived urethane groups owing to the steric hindrance of the isophorone diisocyanate group promoted the dynamics of the networks. The key component to the synthesis of PPOU was 2,6-diacetylpyridine dioxime-urethane, where 2,6-diacetylpyridine dioxime functioned as a chain extender to introduce dynamic oxime-urethane bonds and hydrogen bonds into the polymer. Furthermore, 2,6-diacetylpyridine dioxime functioned as a ligand and provided three N atoms, *i.e.*, one pyridyl N and two oximido N, for coordination with the metal ions. The third step in the synthesis of Fe-PPOU involved the dissolution of PPOU in acetone and the addition of ferric chloride ($FeCl_3$). This resulted in the formation of an Fe-(2,6-diacetylpyridine dioxime)-urethane coordination complex comprising two types of metal-coordination bonds: Fe–$N_{oximido}$ and Fe–$N_{pyridyl}$. The dynamic crosslinking points formed by the metal-coordination bonds optimized the mechanical properties and promoted the self-healing performance of the material. The synthesized Fe-PPOU comprised hydrogen bonds, oxime-urethane bonds, Fe–$N_{oximido}$ bonds, and Fe–$N_{pyridyl}$ bonds. The synergistic effect of the integration of septuple dynamic bonds in one chemical group resulted in not only outstanding mechanical properties but also room-temperature spontaneous self-healing.

The structure of PPOU was characterized *via* FTIR spectroscopy in the attenuated total reflectance (ATR) mode and ^{1}H NMR spectroscopy. The FTIR spectra (Figure 2a, b) presents peaks at 3,410, 3,325, and 1,720 cm^{-1} corresponding to the free N–H, hydrogen-bonded N–H, and C=O bonds, respectively. These results indicate the successful formation of urethane groups. The presence of indistinct peaks corresponding to the isocyanate groups at approximately 2,270 cm^{-1} indicates the complete reaction of the monomer, isophorone diisocyanate. The structure of PPOU was verified *via* the analysis of the ^{1}H NMR spectrum (Figure S8). The presence of indistinct peaks corresponding to tetrahydrofuran at 1.85 and 3.76 ppm indicated the complete removal of the solvent. The weight-average molecular weight (M_w) and number-average molecular weight (M_n) of PPOU were measured to be 112 and 93 kDa, respectively, using gel-permeation chromatography.

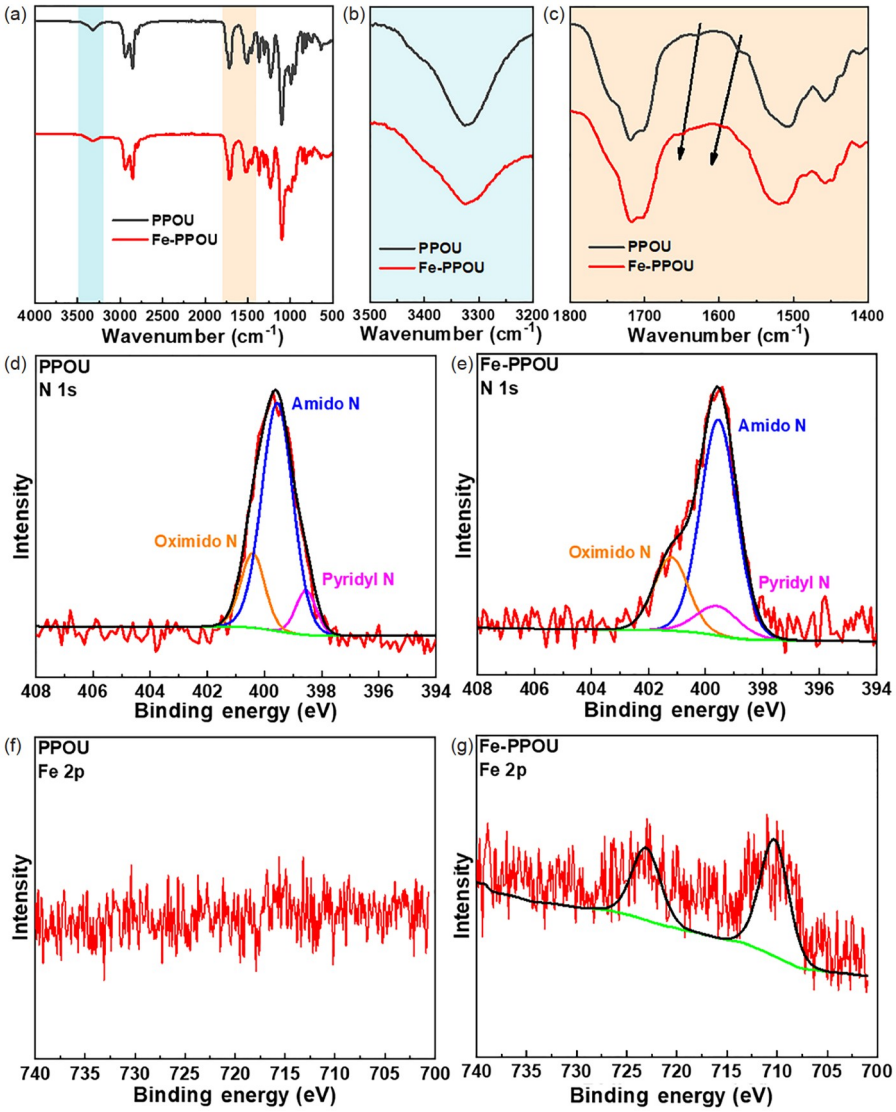

Figure 2 Characterization of PPOU and Fe-PPOU. FTIR spectra of PPOU and Fe-PPOU in the wavenumber range of 500–4,000 cm^{-1} (a), 3,200–3,500 cm^{-1} (b), and 1,400–1,800 cm^{-1} (c). N 1s high-resolution XPS spectra of PPOU (d) and Fe-PPOU (e). Fe 2p high-resolution XPS spectra of PPOU (f) and Fe-PPOU (g) (color online).

The structure of Fe-PPOU was initially characterized *via* FTIR spectroscopy. The overall FTIR spectrum (Figure 2a) of Fe-PPOU was similar to that of PPOU. This indicated that the polymeric structure of PPOU remained unchanged after the introduction of Fe ions. A peak at 1,420 cm^{-1} corresponding to acetone molecular structure was indistinct. This revealed the complete removal of the solvent (acetone). Therefore, the self-healing of Fe-PPOU was not induced by the solvent or the residual monomers. The peaks corresponding to the oximido C=N bonds of PPOU at 1,633 cm^{-1} shifted to 1,648 cm^{-1} in the FTIR spectrum of Fe-PPOU (Figure 2c). In addition, the peaks corresponding to the pyridyl C=N bonds of PPOU at 1,572 cm^{-1} shifted to 1,594 cm^{-1} in the FTIR spectrum of Fe-PPOU (Figure 2c). These observations revealed the coordination of oximido N and pyridyl N with the Fe ions. The introduction of Fe ions did not induce any variations in the amide I and II bands of PPOU at 1,701 and 1,510 cm^{-1}, respectively (Figure 2c). This indicates the negligible participation of the urethane group in the coordination with the Fe ions. These results confirmed the structure of the synthesized Fe-PPOU.

The chemical bonding states of PPOU and Fe-PPOU were characterized *via* XPS. The N 1s high-resolution XPS spectrum of PPOU (Figure 2d) presented three N signals corresponding to oximido N, amido N, and pyridyl N at 400.4, 399.6, and 398.5 eV, respectively [51–53]. The peak area ratio of oximido N to pyridyl N was about 2:1. With the introduction of Fe ions, a shift was observed in the signals of oximido N and pyridyl N to 401.2 and 399.6 eV, respectively (Figure 2e). The peak area ratio of oximido N to pyridyl N was still about 2:1, indicating almost all oximido N and pyridyl N participated in the coordination. The coordination

of 2,6-diacetylpyridine diimine moieties and iron ions was 2:1 [54]. So, the coordination number of Fe–$N_{oximido}$ and Fe–$N_{pyridyl}$ was 4 and 2, respectively. However, there were no variations in the signal of amido N, indicating the negligible participation of amido N in the coordination with the Fe ions. The Fe 2p high-resolution XPS spectrum of Fe-PPOU (Figure 2g) presented two signals corresponding to $2p_{1/2}$ and $2p_{3/2}$ of Fe at 723.2 and 710.3 eV, respectively. No peaks attributed to Fe were detected in the XPS spectrum of PPOU (Figure 2f). The results of the XPS analysis were consistent with those of FTIR spectroscopy. Both the results indicated that the three N atoms, *i.e.*, one pyridyl N and two oximido N, of 2,6-diacetylpyridine dioxime in Fe-PPOU coordinated with the Fe ions to form the Fe-(2,6-diacetylpyridine dioxime)-urethane coordination complex.

The thermomechanical behavior of PPOU and Fe-PPOU were investigated by dynamic mechanical analysis (Figure S9). PPOU (−58.7 °C) and Fe-PPOU (−57.8 °C) showed the similar T_g. The point of intersection between storage modulus E'' and loss modulus E' indicates the transition from solid to liquid state. The transition temperatures of PPOU and Fe-PPOU were 43.2 and 74.2 °C, respectively. Tangent delta ≥ 0.3 is a typical standard for excellent damping performance of polymer materials [44]. Interestingly, Fe-PPOU showed the wide temperature range of the tangent delta larger than 0.3 at solid state from −6.7 to 74.2 °C, while that of PPOU was −18.2 to 43.2 °C, suggesting the potential of Fe-PPOU for damping materials.

PPOU and Fe-PPOU were subjected to stress-relaxation tests under a constant strain (10%) at 25 °C using an electronic universal testing machine. Thus, the role of the septuple dynamic bonds integrated in one chemical group was elucidated. The characteristic relaxation time (τ^*) was defined as the time required for G/G_0 to reach $1/e$ (≈0.37), according to the following exponential decay function: $G(t) = G_0\exp(-t/\tau^*)$. Here, the relaxation modulus (G) was normalized to the initial modulus (G_0). The characteristic relaxation time for Fe-PPOU (τ^*=6.7 s) was slightly higher than that for PPOU (τ^*=3.3 s) (Figure 3b). The stress in Fe-PPOU and PPOU relaxed to 7% and 2%, respectively, of the initial stress with the increase in the relaxation time to 1,000 s, indicating the crosslinking effect of Fe-(2,6-diacetylpyridine dioxime)-urethane coordination complex.

The Arrhenius equation was applied to deduce the apparent activation energies (E_a) from the results of the temperature-dependent stress relaxation tests. The E_a of Fe-PPOU (93.3 kJ mol^{-1}) was significantly higher than that of PPOU (51.7 kJ mol^{-1}) (Figures S10, S11). This indicated the higher stability of the networks in Fe-PPOU as compared with that of the networks in PPOU. The presence of highly stable networks in Fe-PPOU is ascribed to the repeated dissociation and reformation of dynamic crosslinking points, which comprised septuple dynamic bonds in one chemical group, during the network rearrangement. These dynamic crosslinking points originated from the Fe-(2,6-diacetylpyridine dioxime)-urethane coordination complex in Fe-PPOU, and their existence optimized the mechanical properties of the polymer.

The dynamic crosslinking points comprised septuple dynamic bonds in one chemical group, and their presence increased the ultimate tensile strength of the resultant hybrid networks. Furthermore, the dissipation of energy *via* the rupture of the dynamic crosslinking points during stretching induced an increase in the toughness. The ultimate tensile strength of Fe-PPOU (11.9±0.7 MPa) was four times more than that of PPOU (2.5±0.2 MPa) (Figure 3c), while the maximum elongation of Fe-PPOU (2,172%±18%) was 1.6 times that of PPOU (1,330%±65%). The toughness of Fe-PPOU (139.8±18.2 MJ m^{-3}) was 6 times more than that of PPOU (23.1±2.3 MJ m^{-3}) and exceeded the toughness of all the reported room-temperature spontaneously self-healing polymers (Figure 3g) [1,13,22–50]. The strength and the number of coordination bonds are closely related to the mechanical properties of polymers. Strong coordination bonds are generally beneficial to the tensile strength of polymers. However, a large number of strong coordination bonds would increase the number of crosslinking points in the networks, thereby limiting the maximum elongation and toughness of polymers. In Fe-PPOU, an appropriate number of strong coordination bonds were integrated in a limited number of crosslinking points, which were conducive to the maximum elongation and toughness of the polymer. At the same time, a part of the polymer chains in Fe-PPOU were folded owing to the newly formed Fe-(2,6-diacetylpyridine dioxime)-urethane coordination complex; thus, additional hidden lengths were generated. These hidden lengths were released under stretching *via* the dynamic dissociation and reassociation of multiple reversible bonds (Figure 3a). The dissipation of substantial energy during both dissociation and reassociation resulted in a significant increase in the toughness.

In addition to the superior mechanical properties, as mentioned above, Fe-PPOU showed the potential for energy dissipation materials. Energy dissipation corresponds to the ability of materials to convert mechanical energy to thermal energy, which is crucial for many applications such as automobile and construction industry. We performed cyclic tensile tests to demonstrate the damping performance of Fe-PPOU (Figure 3d). The area of the hysteresis loop corresponded to the energy dissipated during the cyclic tensile tests. Damping capacity was defined as the ratio of the dissipated energy and the loading energy [55,56]. With the strain of cyclic tensile tests increased from 100% to 1,500%, the damping capacities of Fe-PPOU were increased from 63.2% to 81.2% with energy dissipation increased from 0.8 to 58.8 MJ m^{-3} (Figure 3e), which was the highest reported

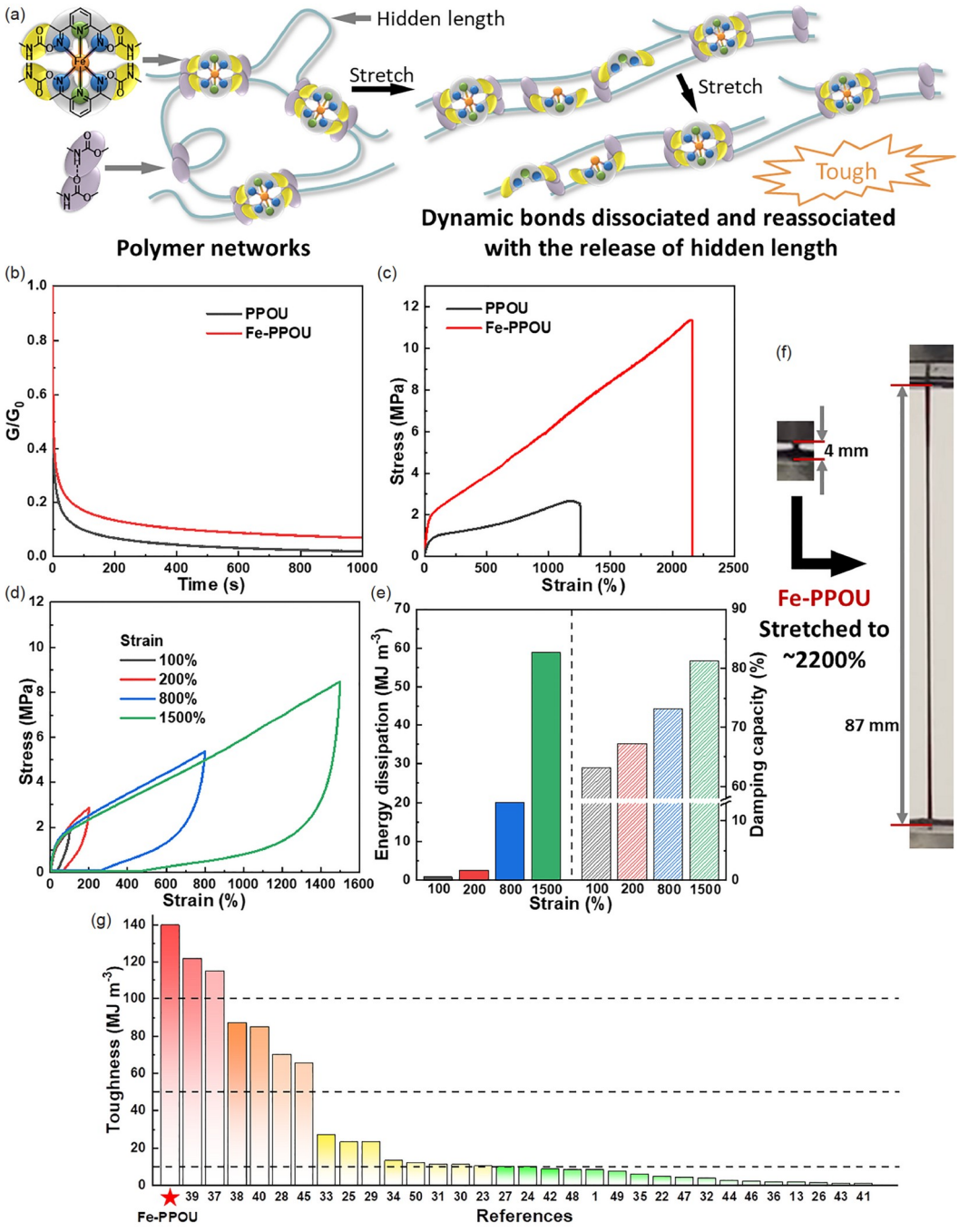

Figure 3 Mechanical properties of Fe-PPOU. (a) Schematic description of the proposed mechanisms for the energy dissipation in Fe-PPOU during stretching. (b) Stress-relaxation curves of PPOU and Fe-PPOU under 10% strain at 25 °C. (c) Typical tensile stress-strain curves of PPOU and Fe-PPOU. (d) Cyclic tensile curves of Fe-PPOU under different maximum strains. (e) Energy dissipation and damping capacity of Fe-PPOU calculated from the cyclic tensile curves under different maximum strains. (f) Photographs of the Fe-PPOU strip before and after stretching. (g) Comparison of the toughness of Fe-PPOU with that of the previously reported room-temperature spontaneously self-healing polymers (color online).

value for room-temperature spontaneously self-healing polymers [1,22,24–26,28,30,31,35,37–40,42–49]. In the initial loading stage, the non-covalent bonds including relatively weak hydrogen bonds would likely break first, and then metal coordination bonds were reversibly broken, and the hidden length of the polymer chain was released. The dynamic crosslinking points were broken and then re-formed at the new positions. In the large stretching, the covalent bonds would also dynamically dissociate. The dynamic re-association of all septuple dynamic bonds led to a large energy dissipation capacity resulting in high toughness of Fe-PPOU.

The self-healing properties of Fe-PPOU were initially evaluated *via* a scratch recovery test. The Fe-PPOU film was

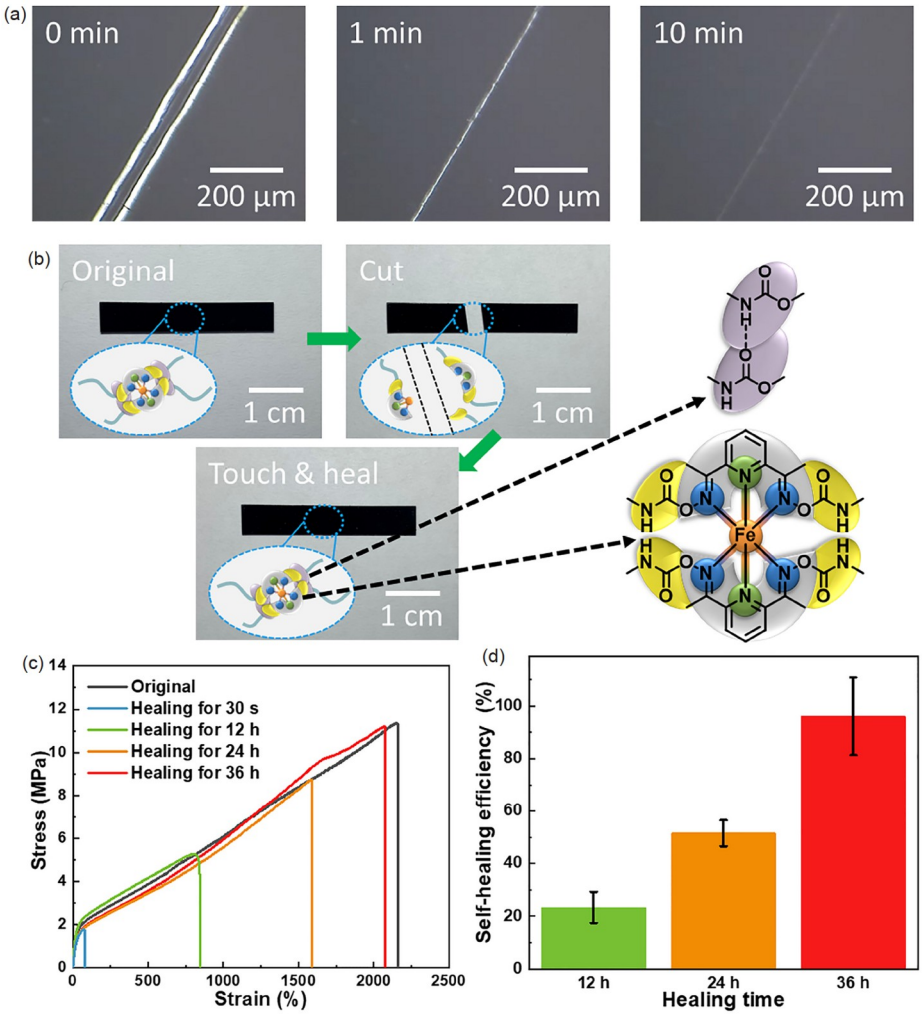

Figure 4 Self-healing properties of Fe-PPOU. (a) Microscopic images of the self-healing process for a scratch (width: 40 μm) on the Fe-PPOU film. (b) Schematics of molecular evolution and digital photographs of the self-healing process of the Fe-PPOU strip. (c) Typical tensile stress-strain curves of the original and healed (specified healing durations at 25 °C without additional stimulation) Fe-PPOU. (d) Self-healing efficiency of the toughness of Fe-PPOU under different healing durations at 25 °C without additional stimulation (color online).

scratched with a blade (width=40 μm) and observed under an optical microscope at 25 °C (Figure 4a). The scratches became inconspicuous within 10 min, thereby indicating the excellent room-temperature spontaneously self-healing ability of Fe-PPOU. Subsequently, the self-healing properties of the bulk materials were evaluated. The strips were cut, and the individual cross sections were then brought in contact to heal. The mechanical properties of the strips after healing were examined after placement at 25 °C for a specific period without additional stimulation (Figure 4b and Figure S12). The introduction of iron ions significantly improved healing efficiency. The instant (after only 30 s of healing) healed tensile strength of Fe-PPOU (1.6±0.3 MPa) was much higher than that of PPOU (1.2±0.1 MPa) and surpassed the original tensile strength of numerous recently reported room-temperature self-healing polymers [22,35,37,41,42,44,46,48]. Furthermore, the tensile stress-strain curves of the same Fe-PPOU spline after three times of instant self-healing were similar (Figure S13), indicating the multiple self-healing excellent performance of Fe-PPOU. There was a gradual increase in the tensile strength, ultimate elongation and toughness of Fe-PPOU with the increase in the healing time (Figure 4c). The self-healing efficiency of the toughness of Fe-PPOU reached 23.4%±5.9%, 51.7% ±5.0%, and 96.1%±14.7% after 12, 24, and 36 h of healing, respectively (Figure 4d), likely due to the gradual re-formation of hydrogen, metal-coordination, and oxime-urethane bonds. To further understand the dynamic networks, master curves were constructed for PPOU and Fe-PPOU at a reference temperature of 25 °C (Figure S14). The point of intersection between storage modulus (G') and loss modulus (G'') indicated the transition of networks from an elastic state to a viscous state. After being coordinated with iron ions, the intersection of Fe-PPOU (0.0047 rad s^{-1}) was moved toward the lower frequency, compared with PPOU (0.0409 rad s^{-1}). The result was ascribed to the dynamic crosslinking by Fe-

(2,6-diacetylpyridine dioxime)-urethane coordination complex. Interestingly, the curves of PPOU and Fe-PPOU showed similar trends, and there was no obvious step. These results indicated that the multiple dynamic bonds in Fe-PPOU may have a synergistic effect on the self-healing in the time scale of the experiments. The healed toughness of Fe-PPOU reached up to 134.3±20.6 MJ m^{-3} within 36 h of healing, which is significantly higher than the toughness of all the reported room-temperature spontaneously self-healing polymers [1,13,22–50]. In addition, Fe-PPOU was cut into pieces and then a flat film was obtained by hot pressing (Figure S15), indicating the good processability of Fe-PPOU.

In order to further study the effect of iron ions on the properties of the polymers, we prepared 0.5Fe-PPOU with half of the Fe-ion amount of Fe-PPOU (Figure S16). The introduction of iron ions significantly enhanced the tensile strength (2.5±0.2 MPa for PPOU, 6.2±0.5 MPa for 0.5Fe-PPOU, 11.9±0.7 MPa for Fe-PPOU) and toughness (23.1 ±2.3 MJ m^{-3} for PPOU, 54.9±5.9 MJ m^{-3} for 0.5Fe-PPOU, 139.8±18.2 MJ m^{-3} for Fe-PPOU) of the polymers. Although the introduction of iron ions limited the speed of self-healing, the final healed tensile strength (2.6±0.2 MPa for PPOU, 5.9 ±0.3 MPa for 0.5Fe-PPOU, 12.0±1.1 MPa for Fe-PPOU) and toughness (21.2±2.1 MJ m^{-3} for PPOU, 51.8±2.4 MJ m^{-3} for 0.5Fe-PPOU, 134.3±20.6 MJ m^{-3} for Fe-PPOU) were significantly improved.

4 Conclusions

The present study demonstrated a room-temperature spontaneously self-healing polymer, Fe-PPOU, with an unprecedented toughness of 139.8 MJ m^{-3}. To the best of our knowledge, the present study is the first to demonstrate the integration of septuple dynamic bonds (two hydrogen bonds, two oxime-urethane bonds, two Fe–$N_{oximido}$ bonds, and one Fe–$N_{pyridyl}$ bond) into one chemical group for the fabrication of high-performance polymers. The synergistic effect of the integration of multiple dynamic bonds in one chemical group optimized the mechanical and self-healing properties of the polymer. As a result, the mechanical and self-healing properties of Fe-PPOU were simultaneously optimized. This molecular design is versatile. Optical, electronic, magnetic, and biological properties can be incorporated in the synthesized polymer by replacing the central metal ions (Fe^{3+}) with lanthanide metal ions (Eu^{3+} and Tb^{3+}) and other physiologically relevant metal ions (Mg^{2+} and Zn^{2+}). The properties of the polymer can also be diversified by replacing the ligand, 2,6-diacetylpyridine dioxime, with other organic ligand groups. The present work demonstrated a novel strategy for the fabrication of high-performance functional self-healing materials.

Acknowledgements This work was supported by the National Key Research and Development Program of China (2021YFC2101804, 2021YFC2101802), the National Natural Science Foundation of China (52173117, 51733002, 52073049, 21991123), the Belt & Road Young Scientist Exchanges Project of Science and Technology Commission Foundation of Shanghai (20520741000), the Natural Science Foundation of Shanghai (20ZR1402500), Shanghai Belt and Road Joint Laboratory of Advanced Fiber and Low-dimension Materials (Donghua University) (18520750400), the Science and Technology Commission of Shanghai Municipality (20DZ2254900) and the Fundamental Research Funds for the Central Universities, DHU Distinguished Young Professor Program (LZA2019001).

Conflict of interest The authors declare no conflict of interest.

Supporting information The supporting information is available online at http://chem.scichina.com and http://link.springer.com/journal/11426. The supporting materials are published as submitted, without typesetting or editing. The responsibility for scientific accuracy and content remains entirely with the authors.

1 Cordier P, Tournilhac F, Soulié-Ziakovic C, Leibler L. *Nature*, 2008, 451: 977–980
2 Toohey KS, Sottos NR, Lewis JA, Moore JS, White SR. *Nat Mater*, 2007, 6: 581–585
3 Zhang MQ, Rong MZ. *Sci China Chem*, 2012, 55: 648–676
4 Sun L, Huang H, Ding Q, Guo Y, Sun W, Wu Z, Qin M, Guan Q, You Z. *Adv Fiber Mater*, 2021, https://doi.org/10.1007/s42765-42021-00086-42768
5 Wang S, Urban MW. *Nat Rev Mater*, 2020, 5: 562–583
6 Wu T, Gray E, Chen B. *J Mater Chem C*, 2018, 6: 6200–6207
7 Qian S, Sun S, Wang Y, Li Z, Lin H. *Sci China Chem*, 2019, 62: 1601–1618
8 Zhang L, You Z. *Chin J Polym Sci*, 2021, 39: 1281–1291
9 Wei P, Chen T, Chen G, Liu H, Mugaanire IT, Hou K, Zhu M. *ACS Appl Mater Interfaces*, 2020, 12: 3068–3079
10 Li CH, Zuo JL. *Adv Mater*, 2019, 31: 1903762
11 Zhang ZP, Rong MZ, Zhang MQ. *Prog Polym Sci*, 2018, 80: 39–93
12 Chakma P, Konkolewicz D. *Angew Chem Int Ed*, 2019, 58: 9682–9695
13 Ying H, Zhang Y, Cheng J. *Nat Commun*, 2014, 5: 3218
14 Liu WX, Yang Z, Qiao Z, Zhang L, Zhao N, Luo S, Xu J. *Nat Commun*, 2019, 10: 4753
15 Zhao J, Xu R, Luo G, Wu J, Xia H. *Polym Chem*, 2016, 7: 7278–7286
16 Ji S, El Mard H, Smet M, Dehaen W, Xu H. *Sci China Chem*, 2017, 60: 1191–1196
17 Chen W, Zhen X, Wu W, Jiang X. *Sci China Chem*, 2020, 63: 648–664
18 Chen X, Dam MA, Ono K, Mal A, Shen H, Nutt SR, Sheran K, Wudl F. *Science*, 2002, 295: 1698–1702
19 Burnworth M, Tang L, Kumpfer JR, Duncan AJ, Beyer FL, Fiore GL, Rowan SJ, Weder C. *Nature*, 2011, 472: 334–337
20 Yanagisawa Y, Nan Y, Okuro K, Aida T. *Science*, 2018, 359: 72–76
21 Bao C, Jiang YJ, Zhang H, Lu X, Sun J. *Adv Funct Mater*, 2018, 28: 1800560
22 Zhang L, Liang J, Jiang C, Liu Z, Sun L, Chen S, Xuan H, Lei D, Guan Q, Ye X, You Z. *Natl Sci Rev*, 2021, 8: nwaa154
23 Chen Y, Kushner AM, Williams GA, Guan Z. *Nat Chem*, 2012, 4: 467–472
24 Wu J, Cai LH, Weitz DA. *Adv Mater*, 2017, 29: 1702616
25 Wang Y, Liu X, Li S, Li T, Song Y, Li Z, Zhang W, Sun J. *ACS Appl Mater Interfaces*, 2017, 9: 29120–29129
26 Rao YL, Chortos A, Pfattner R, Lissel F, Chiu YC, Feig V, Xu J, Kurosawa T, Gu X, Wang C, He M, Chung JW, Bao Z. *J Am Chem Soc*, 2016, 138: 6020–6027
27 Mozhdehi D, Ayala S, Cromwell OR, Guan Z. *J Am Chem Soc*, 2014,

136: 16128–16131
28 Miwa Y, Kurachi J, Kohbara Y, Kutsumizu S. *Commun Chem*, 2018, 1: 5
29 Zhang J, Huo M, Li M, Li T, Li N, Zhou J, Jiang J. *Polymer*, 2018, 134: 35–43
30 Deng Y, Zhang Q, Feringa BL, Tian H, Qu DH. *Angew Chem Int Ed*, 2020, 59: 5278–5283
31 Liu J, Tan CSY, Yu Z, Li N, Abell C, Scherman OA. *Adv Mater*, 2017, 29: 1605325
32 Mei JF, Jia XY, Lai JC, Sun Y, Li CH, Wu JH, Cao Y, You XZ, Bao Z. *Macromol Rapid Commun*, 2016, 37: 1667–1675
33 Kim SM, Jeon H, Shin SH, Park SA, Jegal J, Hwang SY, Oh DX, Park J. *Adv Mater*, 2018, 30: 1705145
34 Rekondo A, Martin R, Ruiz de Luzuriaga A, Cabañero G, Grande HJ, Odriozola I. *Mater Horiz*, 2014, 1: 237–240
35 Yuan WQ, Liu GL, Huang C, Li YD, Zeng JB. *Macromolecules*, 2020, 53: 9847–9858
36 Cash JJ, Kubo T, Bapat AP, Sumerlin BS. *Macromolecules*, 2015, 48: 2098–2106
37 Yan X, Liu Z, Zhang Q, Lopez J, Wang H, Wu HC, Niu S, Yan H, Wang S, Lei T, Li J, Qi D, Huang P, Huang J, Zhang Y, Wang Y, Li G, Tok JBH, Chen X, Bao Z. *J Am Chem Soc*, 2018, 140: 5280–5289
38 Zhang L, Liu Z, Wu X, Guan Q, Chen S, Sun L, Guo Y, Wang S, Song J, Jeffries EM, He C, Qing FL, Bao X, You Z. *Adv Mater*, 2019, 31: 1901402
39 Li Y, Li W, Sun A, Jing M, Liu X, Wei L, Wu K, Fu Q. *Mater Horiz*, 2021, 8: 267–275
40 Wang H, Yang Y, Nishiura M, Higaki Y, Takahara A, Hou Z. *J Am Chem Soc*, 2019, 141: 3249–3257
41 Gao G, Yang F, Zhou F, He J, Lu W, Xiao P, Yan H, Pan C, Chen T, Wang ZL. *Adv Mater*, 2020, 32: 2004290
42 Yang J, Zhang Z, Yan Y, Liu S, Li Z, Wang Y, Li H. *ACS Appl Mater Interfaces*, 2020, 12: 13239–13247
43 Wang H, Liu H, Cao Z, Li W, Huang X, Zhu Y, Ling F, Xu H, Wu Q, Peng Y, Yang B, Zhang R, Kessler O, Huang G, Wu J. *Proc Natl Acad Sci USA*, 2020, 117: 11299–11305
44 Cao PF, Li B, Hong T, Townsend J, Qiang Z, Xing K, Vogiatzis KD, Wang Y, Mays JW, Sokolov AP, Saito T. *Adv Funct Mater*, 2018, 28: 1800741
45 Wang D, Xu JH, Chen JY, Hu P, Wang Y, Jiang W, Fu JJ. *Adv Funct Mater*, 2019, 30: 1907109
46 Liu Z, Zhang L, Guan Q, Guo Y, Lou J, Lei D, Wang S, Chen S, Sun L, Xuan H, Jeffries EM, He C, Qing F, You Z. *Adv Funct Mater*, 2019, 29: 1901058
47 Li CH, Wang C, Keplinger C, Zuo JL, Jin L, Sun Y, Zheng P, Cao Y, Lissel F, Linder C, You XZ, Bao Z. *Nat Chem*, 2016, 8: 618–624
48 Zhang Q, Niu S, Wang L, Lopez J, Chen S, Cai Y, Du R, Liu Y, Lai JC, Liu L, Li CH, Yan X, Liu C, Tok JBH, Jia X, Bao Z. *Adv Mater*, 2018, 30: 1801435
49 Wang T, Zhang Y, Liu Q, Cheng W, Wang X, Pan L, Xu B, Xu H. *Adv Funct Mater*, 2018, 28: 1705551
50 Susa A, Bose RK, Grande AM, van der Zwaag S, Garcia SJ. *ACS Appl Mater Interfaces*, 2016, 8: 34068–34079
51 Fan J, Huang J, Gong Z, Cao L, Chen Y. *ACS Appl Mater Interfaces*, 2020, 13: 1135–1144
52 Wu H, Rondeau-Gagné S, Chiu Y, Lissel F, To JWF, Tsao Y, Oh JY, Tang B, Chen W, Tok JB, Bao Z. *Adv Electron Mater*, 2018, 4: 1800239
53 Gómez-Martínez M, Baeza A, Alonso DA. *Catalysts*, 2017, 7: 94
54 Chiericato G Jr., Arana CR, Casado C, Cuadrado I, Abruña HD. *Inorg Chim Acta*, 2000, 300-302: 32–42
55 Dou Y, Wang ZP, He W, Jia T, Liu Z, Sun P, Wen K, Gao E, Zhou X, Hu X, Li J, Fang S, Qian D, Liu Z. *Nat Commun*, 2019, 10: 5293
56 Zhang Z, Cheng L, Zhao J, Zhang H, Zhao X, Liu Y, Bai R, Pan H, Yu W, Yan X. *J Am Chem Soc*, 2021, 143: 902–911